Chemical Engineering Journal 239 (2014) 114–122

Contents lists available at ScienceDirect

Chemical Engineering Journal

journal homepage: www.elsevier.com/locate/cej

Synergistic effect of iron doped ordered mesoporous carbon on adsorption-coupled reduction of hexavalent chromium and the relative mechanism study

Lin Tang [a,b,*], Gui-De Yang [a,b], Guang-Ming Zeng [a,b,*], Ye Cai [a,b], Si-Si Li [a,b], Yao-Yu Zhou [a,b], Ya Pang [a,b], Yuan-Yuan Liu [a,b], Yi Zhang [a,b], Brandon Luna [c]

[a] *College of Environmental Science and Engineering, Hunan University, Changsha 410082, PR China*
[b] *Key Laboratory of Environmental Biology and Pollution Control, Hunan University, Ministry of Education, Changsha 410082, PR China*
[c] *Department of Chemical Engineering, Columbia University, New York, NY 10027, United States*

HIGHLIGHTS

- Iron doped ordered mesoporous carbon (Fe/CMK-3) was applied as a novel remediation material to remove hexavalent chromium (Cr(VI)).
- A high capacity for the removal of Cr(VI) was observed.
- Cr(VI) removal was an adsorption-coupled reduction process by Fe/CMK-3.
- Fe/CMK-3 showed good magnetic separation performance and excellent reproducibility.

GRAPHICAL ABSTRACT

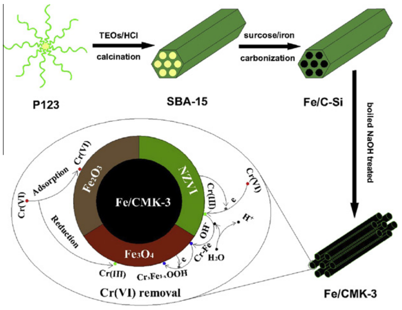

ARTICLE INFO

Article history:
Received 30 October 2013
Accepted 31 October 2013
Available online 15 November 2013

Keywords:
Iron doped ordered mesoporous carbon
Hexavalent chromium
Adsorption
Reduction
Magnetic separation

ABSTRACT

In this study, a magnetic iron nanoparticles doped ordered mesoporous carbon (Fe/CMK-3) was successfully prepared for highly effective removal of Cr(VI). The resultant carbon material maintained ordered mesostructure, high surface area of 679.4 $m^2 g^{-1}$ with 4.42 wt% magnetic nanoparticles (Fe^0, Fe_3O_4 and λ-Fe_2O_3) inside, and excellent magnetic property. Batch experiments were conducted to investigate the removal performance. Fe/CMK-3 exhibited higher Cr(VI) removal efficiency (~97%), broader pH scope of application and easier separation compared with pristine ordered mesoporous carbon (CMK-3). The kinetics data were well described by pseudo-second-order kinetic model, and Langmuir model fitted the sorption isotherms commendably. Moreover, the Cr loaded Fe/CMK-3 could be regenerated by 0.01 mol L^{-1} NaOH solution, and the removal capacity decreased by ~22% in the seventh cycle. X-ray photoelectron spectroscopy (XPS) analysis demonstrated that the Cr(VI) removal was a adsorption and synergistic reduction process owing to trivalent chromium Cr(III) occurring on the surface of Fe/CMK-3. The results suggested that Fe/CMK-3 had potential superiority in removal of Cr(VI) from wastewater.

1. Introduction

Chromium, one of the most widespread heavy metals in the environment, has been widely used in many engineering and chemical industries due to its durabile and aesthetic properties [1]. However, chromium is also considered a major pollutant, even a priority pollutant, by the US EPA [2], since some of its oxidation states are toxic and carcinogenic to humans and animals [3,4]. Cr(VI) is especially poisonous, with toxicity 100 times greater than that of Cr(III). Furthermore, Cr(VI) is also more water-soluble and mobile than Cr(III) in surface water and in groundwater [5]. Thus, it is urgent and necessary to find effective ways to remove Cr(VI) from wastewater.

---

* Corresponding authors at: College of Environmental Science and Engineering, Hunan University, Changsha 410082, PR China. Tel./fax: +86 731 88822778.

E-mail addresses: tanglin@hnu.edu.cn (L. Tang), zgming@hnu.edu.cn (G.-M. Zeng).

1385-8947/$ - see front matter © 2013 Elsevier B.V. All rights reserved.
http://dx.doi.org/10.1016/j.cej.2013.10.104

Recently, various technologies have been employed for Cr(VI) removal, such as ecological remediation [6], chemical precipitation [7], redox [8], and adsorption [9]. Among these techniques, adsorption and reduction are regarded as two most effective and common practices for chromium species removal from effluent associated with proven technological, low-cost advantages and the relatively lower toxicity of trivalent chromium. Various remediation materials involving in adsorption and reduction have been examined for application in Cr(VI) removal, including activated carbon [9], chitosan [10], iron oxide [11] and nanoscale zero-valent iron [12]. However, these materials have some defects, such as low removal capacity [9], aggregation and oxidability [12], limiting the application or treatment effect of these materials.

Nanosized iron particles have stimulated extensive interest for use in wastewater purification in view of their low cost, mild reaction condition and easy separation, and they have been successfully applied to remove organic contaminants [13], heavy metals [14], dyes [15] and so on. But there are still some non-ignorable problems confining their application, including instability, oxidation and aggregation, which lower the particles' reactivity and mobility [16]. To overcome these problems, iron nanoparticles have been immobilized in or on different supports, including active carbon [17], bentonite [18], and multiwalled carbon nanotube [19]. After immobilization, the nanometals could be protected against oxidation and keep their performance.

Besides, carbon nanorods (CMK-3), influential and highly investigated ordered mesoporous carbon possessing unique physical and chemical proprieties such as large surface area, high specific pore volume, hexagonally ordered uniform mesoporous structure, hydrophobicity and thermal stability [20], have shown good performance as adsorptive media [21–23]. In view of the above conditions, it is possible to develop a new adsorbent equipped with improved properties by doping iron nanoparticles on CMK-3. This material could be used as adsorbent with a high effectiveness because of its enhanced ability for adsorption and/or simultaneous reduction of pollutants, and it also can be easily magnetically separated and collected after loading pollutants.

In the present study, a magnetic iron nanoparticles doped ordered mesoporous carbon (Fe/CMK-3) has been successfully prepared using the co-casting method with ordered mesoporous silica SBA-15 as hard template, for use in the removal of Cr(VI) from wastewater. This adsorbent has the crucial adsorptive superiority of ordered mesoporous carbon while adding at the same time the reductive ability and capacity for magnetic separation of iron nanoparticles. The prepared magnetic Fe/CMK-3 was characterized by scanning electron microscopy (SEM), transmission electron microscopy (TEM), Fourier transform infrared (FTIR) analysis, magnetometry, and nitrogen adsorption–desorption isotherms. Furthermore, the relevant parameters such as pH, kinetics, sorption isotherm, and reusability of the composite were investigated to study Fe/CMK-3's sorption-reduction property for Cr(VI) in aqueous solution. The competitive performance from other common salts was also tested. X-ray photoelectron spectroscopy (XPS) analysis was applied to determine the predominant mechanism of the removal of Cr(VI). The resultant composites delivered high efficiency in situ remediation for effluent, and they not only had excellent adsorption capability to target contaminants, but also could reduce Cr(VI) to Cr(III), lowering the chemical toxicity of hexavalent chromium contamination.

2. Materials and methods

2.1. Materials

Pluronic copolymer P123 ($EO_{20}PO_{70}EO_{20}$, EO = ethylene oxide, PO = propylene oxide) was purchased from Sigma–Aldrich (USA), and all reagents used in the experiment were of analytical reagent grade and solutions were prepared with high-purity water (18.25 MΩ cm^{-1}) from a Millipore Milli-Q water purification system.

2.2. Preparation of Fe/CMK-3 and CMK-3

The SBA-15 silica template was prepared according to the process described in the literature [24]. Fe/CMK-3 was synthesized on the basis of a co-impregnation method with slight alterations [25] and the procedure was as follows: 1 mmol $Fe(NO_3)_3 \cdot 9H_2O$ was dissolved into 5 mL aqueous solution containing 1.25 g sucrose and 0.14 g H_2SO_4. Then, the mixed solution was infiltrated into 1 g of calcined SBA-15 template. The resulting mixture was heated in an oven at 100 °C for 6 h and then at 160 °C for another 6 h. In order to obtain fully polymerized sucrose inside the pores of the SBA-15 template, 5 mL of multicomponent aqueous solution containing 0.8 g sucrose and 0.09 g H_2SO_4 were again added to the pre-treated sample and the mixture again underwent the same thermal treatment described above. The material thus obtained was calcined in a nitrogen flow at 900 °C for 6 h with a heating rate of 5 °C min^{-1} to make sucrose carbonized. The resultant product was washed with 1 mol L^{-1} boiling NaOH solution (50 vol% ethanol–50 vol% H_2O) several times to remove the silica template, filtered, washed with 50% ethanol solution until the pH was equivalent to 7, and finally dried at 60 °C for 24 h. Thus, iron doped ordered mesoporous carbon (Fe/CMK-3) was obtained. The detailed preparation process was shown in Fig. 1. For comparison, pristine CMK-3 was also prepared without iron.

2.3. Materials characterization

Scanning electron microscope (SEM) images were obtained on a JEOL JSM-6700. Transmission electron microscopy (TEM) images were obtained on a JEOL-1230 electron microscope operated at 100 kV. Nitrogen adsorption–desorption isotherms were measured on a Micromeritics 2020 analyzer at 77 K. BET analyzes were used to determine the surface area. BJH were analyzes used to derive pore size distribution and calculate the total pore volume. The magnetization measurement was carried out on a vibrating sample magnetometer (VSM) at room temperature. The zeta potentials of the materials were collected using a Malvern ZEN3600 Zetasizer Nano. The surface elemental composition analyzes were proposed based on the X-ray photoelectron spectroscopy (XPS) (Thermo Fisher Scientific, UK) with a resolution of 0.5 eV. Fourier transform

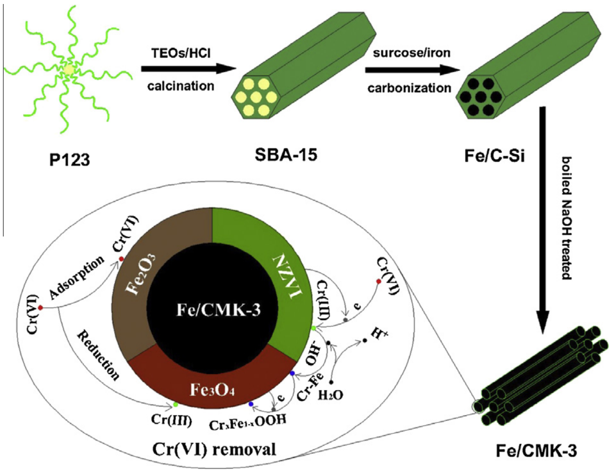

Fig. 1. Schematic representation of Cr(VI) removal by Fe/CMK-3.

infrared (FTIR) spectra of the materials were recorded with a Nicolet NEXUS 670 FTIR spectrometer by the standard KBr disk method.

2.4. Batch experiments

All batch experiments were performed in glass conical flasks undergoing shaking at 150 rpm at room temperature, and the pH values of the solutions were adjusted with 0.1 mol L^{-1} NaOH or 0.1 mol L^{-1} HNO_3 using a pH meter. 10 mg Fe/CMK-3 or CMK-3 was added into 10 mL Cr(VI) solution for each treatment unless otherwise stated. After finishing each experiment, the adsorbents were separated followed by the analysis of residual chromium concentrations in supernatant. The concentration of total Cr in the supernatants was determined by a Perkin–Elmer Analyst 700 atomic absorption spectrophotometer (AAS, Perkin–Elmer, USA), while the Cr(VI) was analyzed using the 1,5-diphenylcarbazide method with a UV–vis spectrophotometer (UV-754 N shanghai, China) at wavelength of 540 nm. The concentration of Cr(III) was determined from the difference between the total and hexavalent chromium concentrations [4]. All the experiments were carried out in duplicate, and the averages results were recorded.

The removal capacity (q) and the removal percentage (R%) of Cr(VI) were calculated by Eqs. (1) and (2), respectively.

$$q = \frac{(c_0 - c_e) \times V}{W} \tag{1}$$

$$R(\%) = \frac{c_0 - c_e}{c_0} \times 100 \tag{2}$$

where q was the adsorption capacity (mg g^{-1}); c_0 and c_e were the initial and residual concentration of Cr(VI) in solution (mg L^{-1}), respectively; V is the volume of Cr(VI) solution (mL), and W is the mass of adsorbent used (mg).

2.5. Desorption and regeneration studies

The feasibility of regenerating Fe/CMK-3 for repeated use was investigated by using sodium hydroxide as stripping agent. Actually, The Cr loaded Fe/CMK-3 was added into 0.1 mol L^{-1} NaOH solution for desorption at 150 rpm at room temperature for 24 h. Then the adsorbent was collected by magnetic separation and washed until neutral for reuse, so that its capacity to remove Cr(VI) could be determined again.

3. Results and discussion

3.1. Characterization of materials

Fig. 2 shows the scanning electron microscope (SEM) and transmission electron microscopy (TEM) images of the pristine CMK-3 and Fe/CMK-3. The SEM images in Fig. 2a and b indicate that the two mesoporous composites had both rodlike morphology, and the average length was about 0.5 μm. From the TEM images of Fig. 2c and d, the ordered stripe-like structures of mesopores were clearly observed for the two mesoporous carbons, but the degree of order was slightly lower for Fe/CMK-3, demonstrating a little deterioration of the ordered mesoporous structure after adding iron. The reasons were that iron precursor, $Fe(NO_3)_3{\cdot}9H_2O$, was decomposed into iron oxide upon heating and was further reduced by carbon to iron particles at high temperatures, arousing some defects in the carbon pore wall and thereby reduced the toughness of carbon pore wall, and at the same time, the reduction of iron oxide into iron also further removed some carbon atoms from

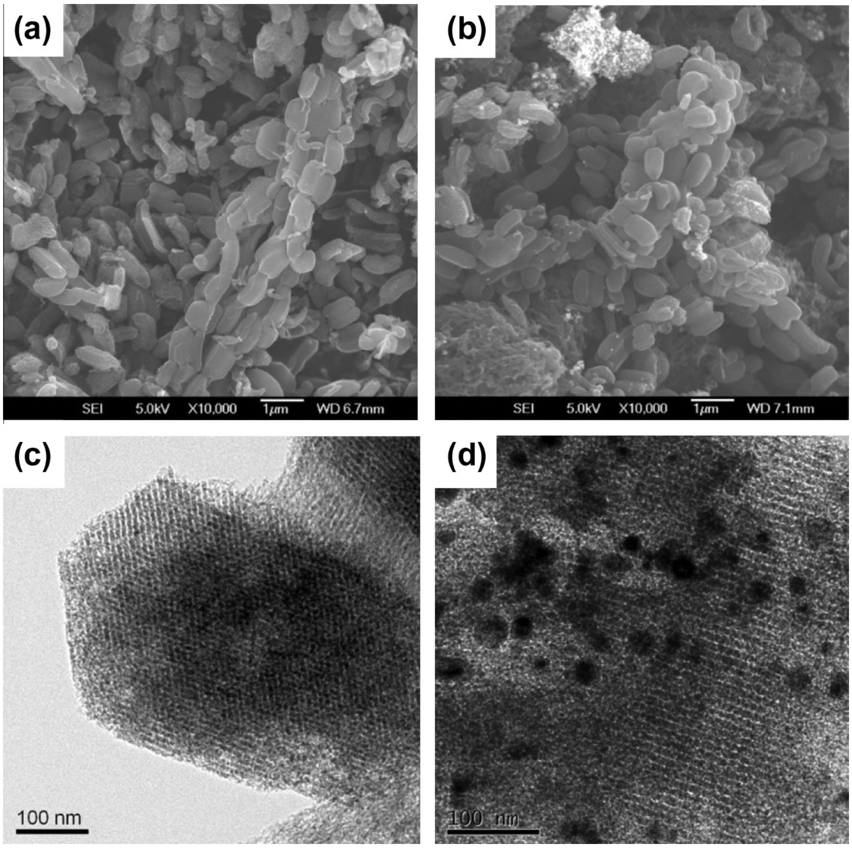

Fig. 2. SEM and TEM images of CMK-3 (a and c) and Fe/CMK-3 (b and d).

the carbon pore wall. Fig. 2d also demonstrated that the nanoparticles with an average diameter about 18 nm were dispersed on the carbon rods matrix, and these nanoparticles may be either Fe_3O_4 or Fe^0 nanoparticles. They were in situ formed when the carbon thermal reduction reaction occurred between iron and carbon during calcination, reducing iron oxides to zero-valent iron or Fe_3O_4.

The isotherm curve (Fig. 3a) showed hysteresis loops in the P/P_0 range 0.6–0.8, indicating that their structures were uniform mesopores. The corresponding pore size distributions calculated from the adsorption branch (Fig. 3b) clearly confirms that the carbons both possessed a pore size distribution centered near 4.75 nm, and uniquely, there occurred a new pore size distribution centered 3.79 nm for Fe/CMK-3, which was not found in the previous study [25]. The new peak might be relevant to the introduction of iron. The introduction of iron also led to a distinct decrease in BET surface area (from 1231.5 to 679.4 $m^2\,g^{-1}$) and in pore volume (from 1.02 to 0.81 $cm^3\,g^{-1}$). This decrease might be due to iron entering into channels, partially occupying or even blocking mesopores.

FTIR spectra for the pristine and iron doping CMK-3 are shown in Fig. 4. For the two carbon materials, the characteristic peak at 3448 cm^{-1} was attributed to the water stuck in the samples, indicating that some hydroxyl groups were formed on the surface of CMK-3 and Fe/CMK-3, and the absorbance band at 1120 cm^{-1} was the C—O stretching vibration in the two carbon materials. The band at around 1640 cm^{-1} also corresponded to the —OH deformation of water or C═O stretching vibration observed in CMK-3 and Fe/CMK-3, which changed a bit due to the introduction of iron. A group of sample-dependent peaks were found at 2365 and 2368 cm^{-1} in CMK-3 and Fe/CMK-3, respectively, which was not found in the previous study, and they could be attributed to C≡C in-line deformation vibrations or carbon dioxide. The band at 572 cm^{-1} that was clearly found in Fe/CMK-3 spectrum (Fig. 4b) was assigned to the Fe—O stretch vibration, demonstrating iron nanoparticles were successfully doped in or on the CMK-3 [26].

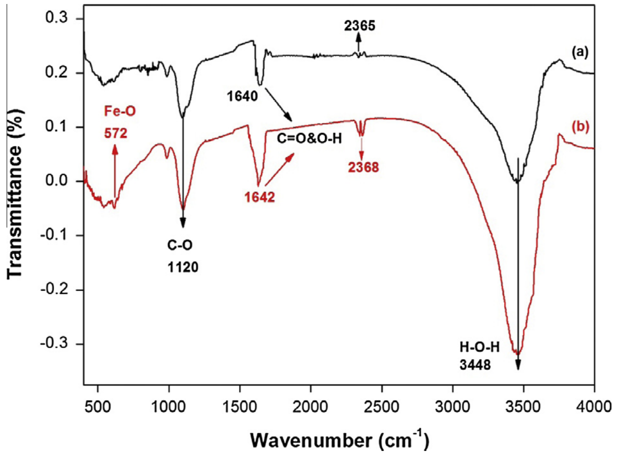

Fig. 4. FTIR spectra of (a) CMK-3 and (b) Fe/CMK-3.

The saturation magnetization strengths (Ms) for Fe/CMK-3 and Cr loaded Fe/CMK-3 were 6.54 and 4.76 emu g^{-1}, respectively (displayed in Fig. 5). The reduction after adsorbing Cr was due largely to a complex reaction occurring between magnetic particles with chromium, which covered the surface of Fe/CMK-3. The magnetic separability of Fe/CMK-3 was tested in aqueous solution by placing a magnet near the glass. The material could be rapidly attracted by the magnet and separated from liquid phase (Fig. 5 inset), demonstrating that Fe/CMK-3 could be promptly magnetically separated [27].

3.2. Effect of solution pH

The zeta potentials of the pristine and iron-doped CMK-3 at different pH values are shown in Fig. 6. The zero point of zeta potentials (pH_{ZPC}) for the two mesoporous composites were at pH 4.8

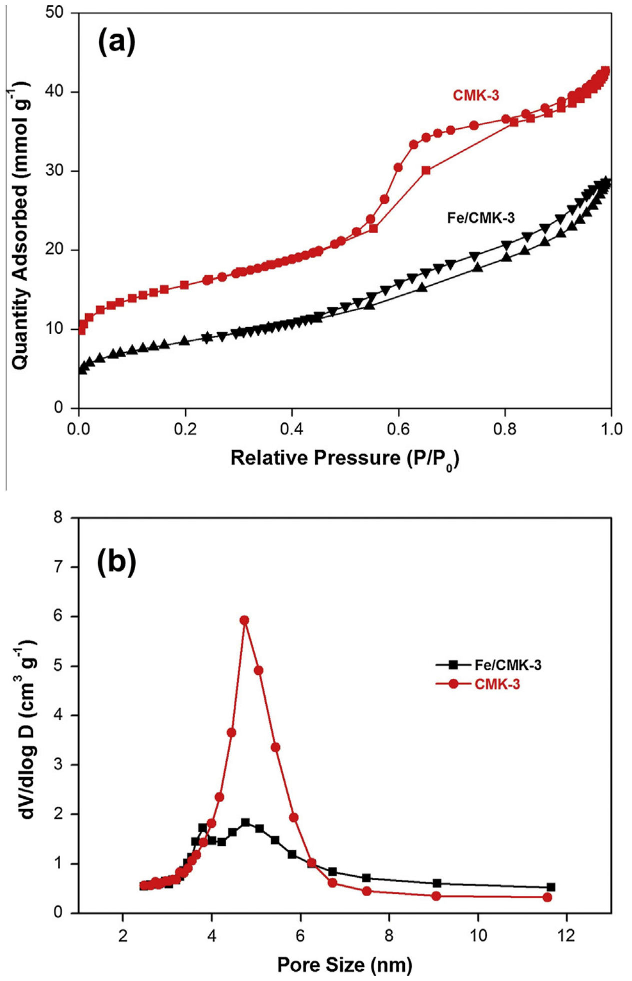

Fig. 3. Nitrogen adsorption–desorption isotherms (a) and pore size distribution (b) of Fe/CMK-3 and CMK-3.

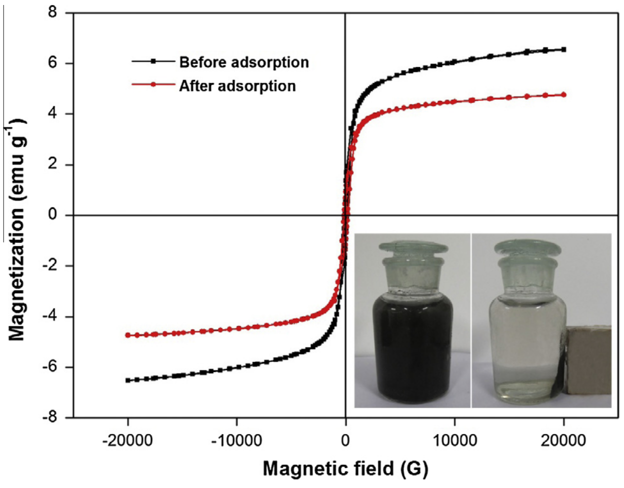

Fig. 5. Magnetization curves of Fe/CMK-3 before and after loading Cr(VI). Inset is a photograph of dispersed Fe/CMK-3 composite in aqueous solution before (left) and after (right) being attracted by an outer magnet.

and 4.2, respectively. The slightly decreasing was associated with the doping of iron. The removal trends of total Cr and Cr(VI) by Fe/CMK-3 and CMK-3 under different initial pH are shown in Fig. 7. The Cr(VI) removal efficiency for Fe/CMK-3 was fairly high in the acidic pH, and it could even reach 97% at pH 5, subsequently, it decreased gradually with increasing of pH. Ultimately, not less than 70% Cr(VI) removal efficiency was still obtained. The pH dependence of heavy metal removal is largely connected with the heavy metal chemistry in the solution and the zeta potentials of the adsorbent [28]. Under the solution pH < $\mathrm{pH_{ZPC}}$, the surface charge on the surface of Fe/CMK-3 was positive. Thus, a significant electrostatic attraction existed between the positively charged surface and the anionic Cr(VI) ions, which was in favor of the adsorption of chromium ions since Cr(VI) existed in different anionic forms in solution, such as $\mathrm{Cr_2O_7^{2-}}$, $\mathrm{HCrO_4^-}$ and $\mathrm{CrO_4^{2-}}$. With increasing of pH, the hydrated surface of Fe/CMK-3 was deprotonated, thereby acquiring a negative charge. Obviously, a negatively charged surface site went against the adsorption of anionic Cr(VI) ions due to electrostatic repulsion. Besides, at alkaline pH, the chromium ions must competed with $\mathrm{OH^-}$ in the solution for the available adsorption sites on the surface or interlayer spaces of Fe/CMK-3, which also hindered the adsorption of Cr(VI).

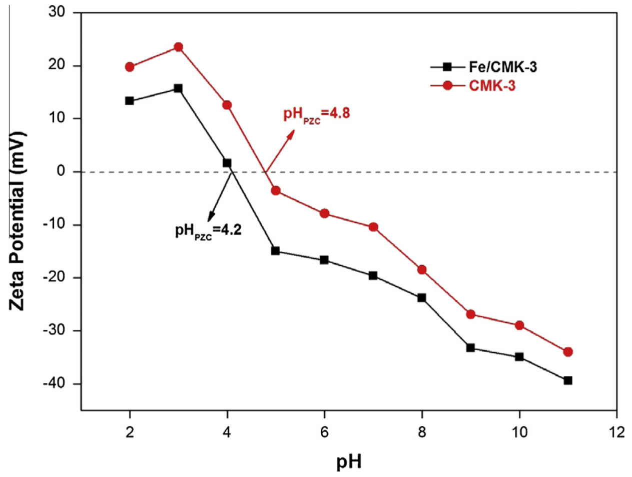

Fig. 6. Zeta potentials of Fe/CMK-3 and CMK-3 at different solution pH.

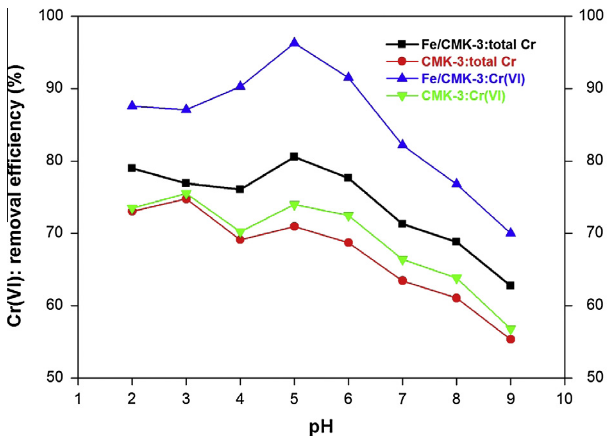

Fig. 7. Effect of pH values on total Cr and Cr(VI) removal by Fe/CMK-3 and CMK-3. Reaction conditions: 100 mg $\mathrm{L^{-1}}$ Cr(VI) removed on Fe/CMK-3 and CMK-3 with concentration of 1 g $\mathrm{L^{-1}}$ at 25 °C, within 3 h.

It still could be found that the total Cr removal efficiency was lower than Cr(VI) for Fe/CMK-3, suggesting that an amount of toxic Cr(VI) was reduced to the less toxic Cr(III) by low oxidation state species of iron on the surface and in the pores of the carbon. The details could be found in Fig. 1. After contacting with Fe/CMK-3, most of Cr(VI) ions were adsorbed on the surface of the adsorbent associating with the available adsorbing sites of ordered mesoporous carbon and magnetic iron nanoparticles. There were also some Cr(VI) participating in the reaction with $\mathrm{Fe^0}$ or $\mathrm{Fe_3O_4}$, generating low toxic Cr(III), further shaping Cr–Fe complexes under the action of hydrone. A possible mechanism for this reduction is proposed in Eqs. (3)–(5):

$$3\mathrm{Fe^0} + \mathrm{CrO_7^{2-}} + 7\mathrm{H_2O} \rightarrow 3\mathrm{Fe^{2+}} + 2\mathrm{Cr(OH)_3} + 8\mathrm{OH^-} \tag{3}$$

$$x\mathrm{Cr^{3+}} + (1-x)\mathrm{Fe^{3+}} + 3\mathrm{H_2O} \rightarrow (\mathrm{Cr}_x\mathrm{Fe}_{1-x})(\mathrm{OH})_3 + 3\mathrm{H^+} \tag{4}$$

$$x\mathrm{Cr^{3+}} + (1-x)\mathrm{Fe^{3+}} + 2\mathrm{H_2O} \rightarrow \mathrm{Cr}_x\mathrm{Fe}_{1-x}\mathrm{OOH} + 3\mathrm{H^+} \tag{5}$$

At the same time, compared with CMK-3, it is more efficiently for Fe/CMK-3 removal of Cr(VI) across a wide pH range. This could be attributed to the conjunct occurrence of Cr(VI) adsorption, reduction and an Fe–Cr complex reaction, thus lowering the concentration of hexavalent chromium in the solution.

Considering the adsorption capacity and the feasibility of actual operation, in the following experiments, initial pH 5.0 was used as the optimum pH.

3.3. Effect of contact time on Cr(VI) removal

The effects of contact time on total Cr and Cr(VI) removal by Fe/CMK-3 and CMK-3 are presented in Fig. 8. The removal capacities of Cr(VI) were observed to increase markedly with increasing contact time from 0 to 30 min for the two mesoporous adsorbents, subsequently, a slight fluctuation occurred in the next time and apparent equilibrium were achieved after about 180 min. The sorption efficiency was obviously improved after doping iron, within the first 30 min adsorption, more than 90% Cr(VI) ions was removed by Fe/CMK-3, while only less than 70% Cr(VI) ions removed by CMK-3. It is worth to note that the capacity for removal of Cr(VI) was improved after the introduction of iron, and the equilibrium adsorption amount reached 97.69 mg $\mathrm{g^{-1}}$ compared with pristine CMK-3, whose equilibrium adsorption amount was 71.59 mg $\mathrm{g^{-1}}$. The above improvements in adsorption rate and adsorption amount indicated that Fe/CMK-3 had potential advantage in Cr(VI) removal.

An adsorption kinetic model was applied to estimate adsorption rate, and to simultaneously research the possible reaction mechanisms of Cr(VI) removal. The pseudo-second-order adsorption model, usually correlative with the behavior over the whole range of adsorption, was utilized to fit the experimental data. The kinetic rate equation is expressed in Eq. (6):

$$\frac{dq_t}{dt} = k(q_e - q_t)^2 \tag{6}$$

where q_e and q_t (mg $\mathrm{g^{-1}}$) are the amounts of removed Cr(VI) at equilibrium and at time t, respectively, k (g $\mathrm{mg^{-1}}$ $\mathrm{min^{-1}}$) is the pseudo-second-order rate constant.

Integrating and applying boundary conditions $t = 0$ to $t = t$, and $q = 0$ to $q = q_t$ gives

$$\frac{t}{q_t} = \frac{1}{kq_e^2} + \frac{t}{q_e} \tag{7}$$

A plot between t/q_t versus t gives the value of the constants k (g $\mathrm{mg^{-1}}$ $\mathrm{min^{-1}}$) and also q_e (mg $\mathrm{g^{-1}}$) can be calculated and given in Table 1. It was found that the linear relationships between t/q_t and t had very high correlation coefficients $R^2 > 0.999$, demonstrating that the removal systems were well fitted using the pseudo-second-order model.

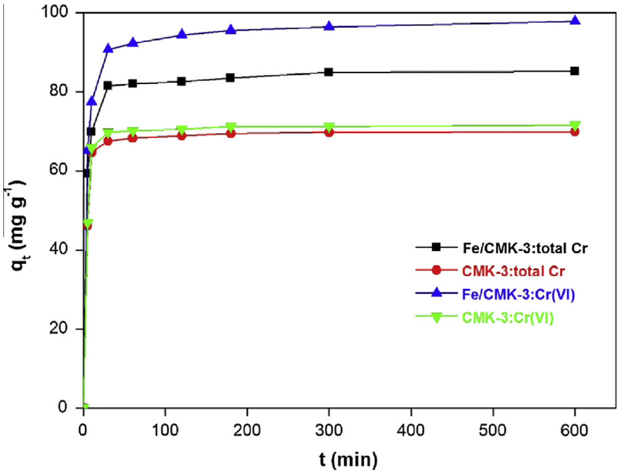

Fig. 8. Effect of contact time on total Cr and Cr(VI) removal by Fe/CMK-3 and CMK-3. Reaction conditions: 100 mg L^{-1} Cr(VI) removed on Fe/CMK-3 and CMK-3 with concentration of 1 g L^{-1} at 25 °C, pH 5.

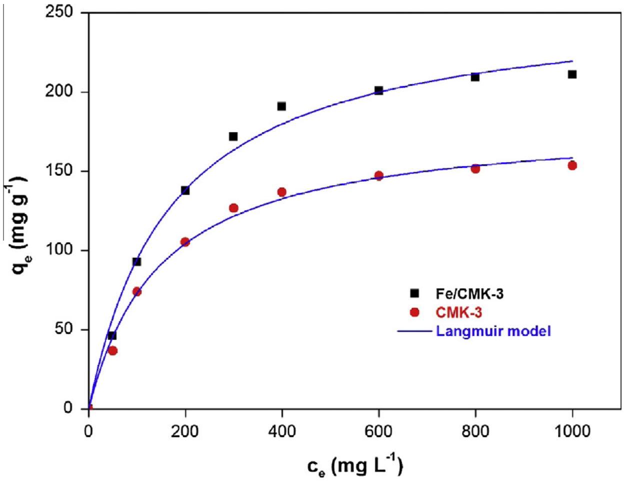

Fig. 9. Adsorption isotherms for Cr(VI) removal onto Fe/CMK-3 and CMK-3 using Langmuir isotherm model. Reaction conditions: different concentrations of Cr(VI) removed on Fe/CMK-3 and CMK-3 with concentration of 1 g L^{-1} at 25 °C, pH 5, within 3 h.

3.4. Sorption isotherms

Fig. 9 showed the sorption isotherms of Cr(VI) on the Fe/CMK-3 and CMK-3. The sorption amounts increased with increasing equilibrium concentrations, and gradually approached the maximum sorption capacities 210.84 and 153.59 mg g^{-1} for Fe/CMK-3 and CMK-3, respectively. In the lower equilibrium concentrations, Cr(VI) can almost be fully adsorbed on the surface of two adsorbents. With the increasing of Cr(VI) equilibrium concentrations, the available adsorption sites gradually decreases. At the same time, the remaining vacant surface sites are also difficult to be occupied because of repulsive forces between the solute ions on the solid and bulk phases, and finally, the equilibrium was arrived.

Adsorption isotherms depict the interaction pathway of pollutants with remediation materials [11]. In the study, two adsorption isothermal models: Langmuir and Freundlich isotherms were used to analyze the experiment data. The Langmuir isotherm model was assumes that the adsorption occurred in a monolayer and all sites were equal, while the Freundlich isotherm model is an empirical formula for describing heterogeneous systems. Their equations are expressed in Eqs. (8) and (9):

$$\text{Langmuir}: \quad q_e = \frac{q_m K_L c_e}{1 + K_L c_e} \tag{8}$$

$$\text{Freundlich}: \quad q_e = K_F c_e^{1/n} \tag{9}$$

where q_e (mg g^{-1}) is the amount of Cr(VI) adsorbed at equilibrium, q_m (mg g^{-1}) is the maximum adsorption capacity, c_e (mg L^{-1}) is the equilibrium solute concentration, K_L (L mg^{-1}) is the Langmuir constant related to adsorption energy, and K_F and n are Freundlich constants and intensity factors, respectively.

The corresponding values of Langmuir and Freundlich isotherm models are also listed in Table 2. It could be observed that the Langmuir isotherm model is more appropriate for the results with the higher correlation coefficient R^2, and it implied that the two mesoporous adsorbents were homogeneous in the liquid phase and the removal of Cr(VI) was similar to monolayer adsorption [14]. Besides, the stability constant (K_L) for removal of Cr(VI) got larger, demonstrating that the bond energy between the surface sites and Cr(VI) was larger for Fe/CMK-3. Comparing the maximum capacity of Cr(VI) removal with the previous study [21,29–33] (shown in Table 3), the prepared mesoporous materials were better than many other absorbents reported in the literature.

Moreover, the separation factor (R_L) was introduced to measure the favorability of Cr(VI) adsorption process. The formula of R_L was expressed as Eq. (10):

$$R_L = \frac{1}{1 + K_L c_e} \tag{10}$$

It was found that $0 < R_L < 1$ because K_L was positive, which made clear that the adsorption of Cr(VI) onto Fe/CMK-3 and CMK-3 was favorable and could be suitable for Langmuir isotherm model.

3.5. Effect of common salts on Cr(VI) removal

Other salts might compete with Cr(VI) for Fe/CMK-3's available binding sites. In this study, four commonly coexisting salts, NaCl, $Ca(NO_3)_2$, Na_2SO_4 and K_3PO_4, were chosen to study the effect on Cr(VI) removal. The results are shown in Fig. 10. NaCl and $Ca(NO_3)_2$ scarcely influenced the removal of Cr(VI), however, the presence of Na_2SO_4 and K_3PO_4 could reduce the materials' capacity of removing Cr(VI) from ~97% to ~70% and ~77%, respectively. The reasons were that Cl^- and NO_3^- were monovalent anions, and they would not or would only very slightly compete for the adsorption sites of Fe/CMK-3. Whereas, for SO_4^{2-} and PO_4^{3-}, they were multivalent anions, possessing similar structures and sizes with $Cr_2O_7^{2-}$, $HCrO_4^-$ and CrO_4^{2-}, and they could compete with Cr(VI) for the available adsorption sites of Fe/CMK-3. Thus, with increasing of

Table 1
Pseudo-second-order model parameters for total Cr and Cr(VI) adsorption on Fe/CMK-3 and CMK-3.

Absorbents	Total Cr			Cr(VI)		
	k (g mg^{-1} min^{-1})	q_e (mg g^{-1})	R^2	k (g mg^{-1} min^{-1})	q_e (mg g^{-1})	R^2
Fe/CMK-3	0.0055	85.32	0.9999	0.0035	97.94	0.9992
CMK-3	0.0108	69.98	0.9998	0.0105	71.68	0.9995

Table 2
Langmuir and Freundlich parameters for Cr(VI) adsorption by Fe/CMK-3 and CMK-3.

Absorbents	Langmuir			Freundlich		
	K_L (L mg^{-1})	q_m (mg g^{-1})	R_1^2	K_F	n	R_2^2
Fe/CMK-3	0.0058	256.86	0.9903	19.02	2.76	0.8773
CMK-3	0.0067	182.03	0.9928	16.2	2.95	0.8752

Table 3
The maximal removal capacities (q_m) of various adsorbents used for Cr(VI) removal.

Adsorbents	q_m (mg g^{-1})	References
Fe^0/Fe_3O_4 nanoparticles	55.64	[29]
Magnetic chitosan 1 (NCIM 3589)	186.15 ± 3.12	[30]
Magnetic chitosan 2 (NCIM 3590)	137.27 ± 4.68	[30]
Magnetized activated carbon	57.19	[31]
Polypyrrole–polyaniline (PPy–PANI) nanofibers	227.22	[32]
NN-sicilia	118.55	[33]
OMC-P	189.39	[21]
OMC-F	128.21	[21]
CMK-3	182.03	This study
Fe/CMK-3	256.86	This study

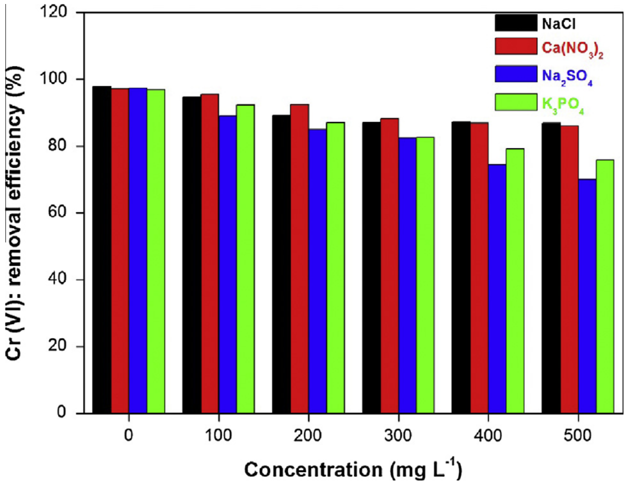

Fig. 10. Effect of different concentrations of NaCl, $Ca(NO_3)_2$, Na_2SO_4 and K_3PO_4 on removal Cr(VI) by Fe/CMK-3. Reaction conditions: 100 mg L^{-1} of Cr(VI) removed on Fe/CMK-3 and CMK-3 with concentration of 1 g L^{-1} at 25 °C, pH 5, within 3 h.

the concentrations of SO_4^{2-} and PO_4^{3-}, the Cr(VI) removal reduced gradually.

3.6. Other heavy metals adsorption

To further explore the adsorption performance of Fe/CMK-3, 800 mg L^{-1} of Zn^{2+}, Cu^{2+}, Cd^{2+} and $Cr_2O_7^{2-}$ were used to study the adsorption efficiency of CMK-3 and Fe/CMK-3, and the results were showed in Table 4. It could be found that the heavy metal ions removal performance of Fe/CMK-3 was better than CMK-3 in the whole (except for Zn^{2+}), which was largely related with more available adsorption sites and suitable size of pores on the surface of ordered mesoporous carbon and magnetic nanoparticles after the introduction of iron.

3.7. Regeneration of Fe/CMK-3

Because of a reversible process of Cr(VI) adsorption onto magnetic material, it was possible to regenerate and reactivate the remediation material to reuse. In the study, the regeneration of Fe/CMK-3 was surveyed using sodium hydroxide desorption and magnet separation. Several successive cycles were shown in Fig. 11. The adsorption efficiency was decreased gradually with the increasing of cycle, but no less than 75% efficiency was obtained in the seventh cycle, demonstrating that Fe/CMK-3 was capable of being regenerated and used repeatedly using sodium hydroxide.

Table 4
The adsorption performance of other heavy metals onto Fe/CMK-3 and CMK-3 (800 mg L^{-1} of Zn^{2+}, Cu^{2+}, Cd^{2+} and $Cr_2O_7^{2-}$ removed on Fe/CMK-3 and CMK-3 with concentration of 1 g L^{-1} at 25 °C, pH 5, within 3 h).

Absorbents	Zn^{2+} (mg g^{-1})	Cu^{2+} (mg g^{-1})	Cd^{2+} (mg g^{-1})	$Cr_2O_7^{2-}$ (mg g^{-1})
Fe/CMK-3	195	215	238	209.4
CMK-3	224	198	210	151.6

3.8. XPS analysis

In order to find out the main mechanisms of Cr(VI) removal by the adsorbents and the change in the elements' chemical or valence states, X-ray photoelectron spectroscopy (XPS) was applied to study the surface chemical compositions of the carbons and the results are presented in Figs. 12 and 13. Fig. 12 shows the whole region scan of the Fe/CMK-3 surface before and after being exposed to the aqueous solution containing 100 mg L^{-1} Cr(VI) at initial pH 5 and 20 °C. For pure Fe/CMK-3, the principal elements at the surface were carbon (79.81%), oxygen (13.64%), iron (4.42%), and silicon (2.13%). The existence of carbon and oxygen composed the main body of the carbon, the silicon came from the template of mesoporous carbons, and the small amounts of iron were added deliberately. A new peak in the banding energy of about 580 eV appeared after contact with Cr(VI) for 3 h, which was attributed to the photoelectron peaks of chromium and indicated the uptake of chromium on the Fe/CMK-3 surface.

Detailed XPS surveys of the regions for Fe2p and Cr2p were showed in Fig. 13. For the chromium spectra shown in Fig. 13a, the photoelectron peaks for the chromium 2p3/2 and 2p1/2 centered at 576.9 and 587.1 eV, respectively, and both were similar to the binding energies of Cr(III)-containing material [4,34]. This data demonstrated that part of adsorbed Cr(VI) anions was reduced to Cr(III) after exposure to Fe/CMK-3. Further analysis suggested that the Cr(III) compound formed at the Fe/CMK-3 surface was $Cr(OH)_3$, not Cr_2O_3. The reason was that chromium 2p3/2 and

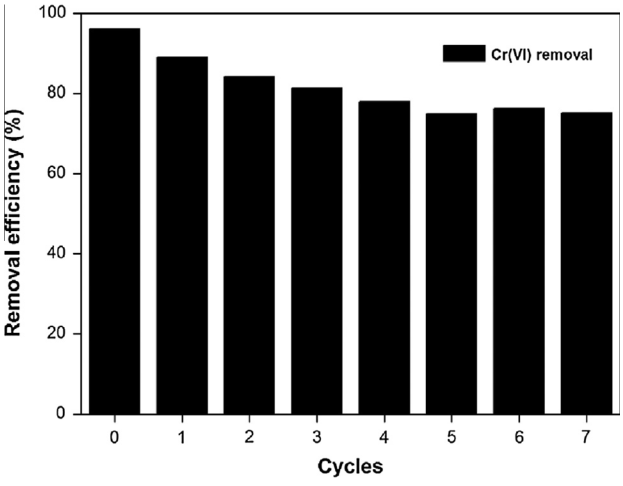

Fig. 11. Seven consecutive adsorption–desorption cycles of Fe/CMK-3 for Cr(VI).

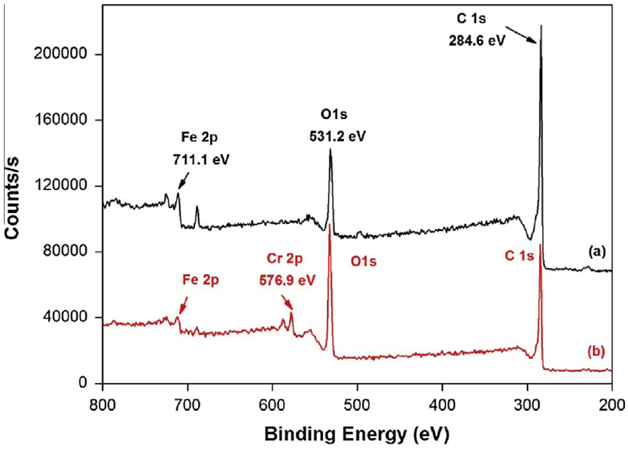

Fig. 12. XPS survey for Fe/CMK-3 before (a) and after (b) reacting with 100 mg L^{-1} Cr(VI).

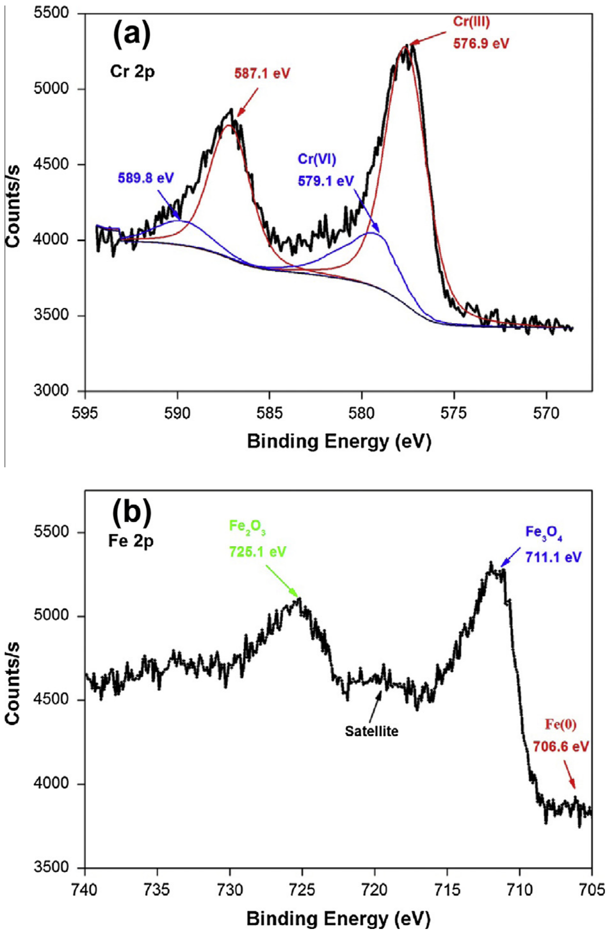

Fig. 13. XPS survey of (a) chromium 2p and (b) iron 2p of Fe/CMK-3 after reacting with 100 mg L^{-1} Cr(VI).

2p1/2 spectra presented in Fig. 13a, could not be reasonably fitted with the binding energies of Cr_2O_3 [35]. The result shows clearly that the Cr(VI) removal process involved the reduction of Cr(VI) into Cr(III) during the sorption. However, no significant bands of Cr(VI) appeared in the XPS spectrum of Fe/CMK-3 loaded with Cr(VI) even though batch adsorption experiments had shown that a mass of Cr(VI) was removed after contact with Fe/CMK-3 (Figs. 7 and 8), which was similar to the previous study [36]. The reason was probable that the reduction of Cr(VI) occurred on the surface of the Fe/CMK-3 material, and the products of reduction were loaded on the surface or combined with iron oxide, hiding the trace of Cr(VI) existence.

For Fe2p spectra (shown in Fig. 13b), where the 711.1 and 725.1 eV binding energy of Fe2p could be assigned to Fe_3O_4 and Fe_2O_3, respectively, according to previous studies [37], and the satellite between two dominant peaks was contributed by Fe^{2+} via a shake-up process [38]. Besides, there was almost no peak corresponding to Fe^0 occurring in Fig. 13b, which might be because the surface Fe^0 of the carbon was oxidized by oxygen and participating in the redox reaction (Cr(VI)–Cr(III)). Furthermore, the amount of oxygen in the total carbon material increased from 13.64% to 33.04% (Fig. 12), demonstrating that hydroxyl was involved with the reduction of Cr(VI), and that Cr(III)–Fe(III) (hydr)oxides precipitation occurred in the reaction [39].

4. Conclusions

In this work, a magnetic iron doped ordered mesoporous carbon was successfully synthesized and applied to remove anionic Cr(VI) in the wastewater. The magnetic composite showed an effective Cr(VI)-removal performance, by combining its adsorption and reduction dual functions. The adsorption efficiency was slightly affected by the solution pH and the maximum Cr(VI) adsorption was found at pH 5. The pseudo-second-order kinetic and Langmuir isotherm models were best able to fit the experimental data. Multivalent anions (SO_4^{2-} and PO_4^{3-}) could hinder Cr(VI) adsorption. Other heavy metals were also commendably adsorbed by Fe/CMK-3. Besides, the adsorbent could be capable of being regenerated and reused using sodium hydroxide. XPS analysis confirmed that Cr(III) and a bit of iron oxide existed on the surface of Fe/CMK-3. The above results present a compelling case that with further development, Fe/CMK-3 might offer an effective treatment to remove Cr(VI) from wastewater in industrial practice.

Acknowledgments

The study was financially supported by Program for the Outstanding Young Talents of China, the National Natural Science Foundation of China (51222805), the Program for New Century Excellent Talents in University from the Ministry of Education of China (NCET-11-0129), Interdisciplinary Research Project of Hunan University, China Scholarship Council (CSC) (2010843195), the Fundamental Research Funds for the Central Universities, Hunan University, and Foundation for the Author of Excellent Doctoral Dissertation of Hunan Province.

References

[1] M. Baikousi, A.B. Bourlinos, A. Douvalis, Th. Bakas, D.F. Anagnostopoulos, J. Tucek, K. Safarova, R. Zboril, M.A. Karakassides, Synthesis and characterization of γ-Fe_2O_3/carbon hybrids and their application in removal of hexavalent chromium ions from aqueous solutions, Langmuir 28 (2012) 3918–3930.

[2] US EPA, Ground Water and Drinking Water, Current Drinking Water Standards, EPA 2011 816-F-02.

[3] Y.J. Li, B.Y. Gao, T. Wu, D.J. Sun, X. Li, B. Wang, F.J. Lu, Hexavalent chromium removal from aqueous solution by adsorption on aluminum magnesium mixed hydroxide, Water Res. 43 (2009) 3067–3075.

[4] Y.Y. Sun, Q.Y. Yue, B.Y. Gao, Y. Gao, Q. Li, Y. Wang, Adsorption of hexavalent chromium on Arundo donax Linn activated carbon amine-crosslinked copolymer, Chem. Eng. J. 217 (2013) 240–247.

[5] H. Shen, Y. Wang, Simultaneous chromium reduction and phenol degradation in a coculture of *Escherichia coli* ATCC 33456 and *Pseudomonas putida* DMP-1, Appl. Environ. Microbiol. 61 (1995) 2754–2758.

[6] Q.X. Zhou, Y.F. Song, Remediation of Contaminated Soils: Principles and Methods, Science Press, China, Beijing, 2004.

[7] X. Zhou, T. Korenaga, T. Takahashi, T. Moriwake, S. Shinoda, A process monitoring/controlling system for the treatment of wastewater containing chromium(VI), Water Res. 27 (1993) 1049–1054.

[8] Y. Pang, G.M. Zeng, L. Tang, Y. Zhang, Y.Y. Liu, X.X. Lei, M.S. Wu, Z. Li, C. Liu, Cr(VI) reduction by *Pseudomonas aeruginosa* immobilized in a polyvinyl alcohol/sodium alginate matrix containing multi-walled carbon nanotubes, Bioresour. Technol. 102 (2011) 10733–10736.

[9] D. Mohan, C.U. Pittman Jr., Activated carbons and low cost adsorbents for remediation of tri- and hexavalent chromium from water, J. Hazard. Mater. 137 (2006) 762–811.

[10] S.X. Li, Y.Q. Lian, J.F. Mai, J.X. Tan, S.J. Hu, W.Q. Xia, W.W. Duan, Removal of hexavalent chromium and turbidity in drinking water by chitosan, Adv. Mater. 433–440 (2012) 793–797.

[11] P. Xu, G.M. Zeng, D.L. Huang, C.L. Feng, S. Hu, M.H. Zhao, C. Lai, Z. Wei, C. Huang, G.X. Xie, Z.F. Liu, Use of iron oxide nanomaterials in wastewater treatment: a review, Sci. Total Environ. 424 (2012) 1–10.

[12] X.Q. Li, J.S. Cao, W.X. Zhang, Stoichiometry of Cr(VI) immobilization using nanoscale zerovalent iron (nZVI): a study with high-resolution X-ray photoelectron spectroscopy (HR-XPS), Ind. Eng. Chem. Res. 47 (2008) 2131–2139.

[13] T. Phenrat, Y.Q. Liu, R.D. Tilton, G.V. Lowry, Adsorbed polyelectrolyte coatings decrease Fe^0 nanoparticle reactivity with TCE in water: conceptual model and mechanisms, Environ. Sci. Technol. 43 (2009) 1507–1514.

[14] Y. Pang, G.M. Zeng, L. Tang, Y. Zhang, Y.Y. Liu, X.X. Lei, Zh. L, J.Ch. Zhang, Zh.F. Liu, Y.Q. Xiong, Preparation and application of stability enhanced magnetic nanoparticles for rapid removal of Cr(VI), Chem. Eng. J. 175 (2011) 222–227.

[15] D.M. Yuna, H.H. Cho, J.W. Jang, J.W. Park, Nano zero-valent iron impregnated on titanium dioxide nanotube array film for both oxidation and reduction of methyl orange, Water Res. 5 (2013) 1858–1866.

[16] T. Phenrat, N. Saleh, K. Sirk, R.D. Tilton, G.V. Lowry, Aggregation and sedimentation of aqueous nanoscale zerovalent iron dispersions, Environ. Sci. Technol. 41 (2006) 284–290.

[17] L.M. Wu, L.B. Liao, G.Ch. Lv, F.X. Qin, Y.J. He, X.Y. Wang, Micro-electrolysis of Cr(VI) in the nanoscale zero-valent iron loaded activated carbon, J. Hazard. Mater. 254–255 (2013) 277–283.

[18] Y.M. Li, J.F. Li, Y.L. Zhang, Mechanism insights into enhanced Cr(VI) removal using nanoscale zerovalent iron supported on the pillared bentonite by macroscopic and spectroscopic studies, J. Hazard. Mater. 227–228 (2012) 211–218.

[19] J. Xu, X.Sh. Lv, J.D. Li, Y.Y. Li, L. Shen, H.Y. Zhou, X.H. Xu, Simultaneous adsorption and dechlorination of 2,4-dichlorophenol by Pd/Fe nanoparticles with multi-walled carbon nanotube support, J. Hazard. Mater. 225–226 (2012) 36–45.

[20] L. Tang, Y.Y. Zhou, G.M. Zeng, Z. Li, Y.Y. Liu, Y. Zhang, G.Q. Chen, G.D. Yang, X.X. Lei, M.S. Wu, A tyrosinase biosensor based on ordered mesoporous carbon–Au/L-lysine/Au nanoparticles for simultaneous determination of hydroquinone and catechol, Analyst 138 (2013) 3552–3560.

[21] T. Chen, T. Wang, D.J. Wang, H.R. Xue, J.Q. Zhao, X.Ch. Ding, Sh.Ch. Wu, J.P. He, Synthesis of ordered large-pore mesoporous carbon for Cr(VI) adsorption, Mater. Res. Bull. 46 (2011) 1424–1430.

[22] N.N. Liu, L.W. Yin, L.Y. Zhang, C.B. Wang, N. Lun, Y.X. Qi, C.X. Wang, Ferromagnetic Ni decorated ordered mesoporous carbons as magnetically separable adsorbents for methyl orange, Mater. Chem. Phys. 131 (2011) 52–59.

[23] J.G. He, K. Ma, J. Jin, Zh.P. Dong, J.J. Wang, R. Li, Preparation and characterization of octyl-modified ordered mesoporous carbon OMC for phenol adsorption, Micropor. Mesopor. Mater. 121 (2009) 173–177.

[24] D. Zhao, Q. Huo, J. Feng, B.F. Chmelka, G.D. Stucky, Nonionic triblock and star diblock copolymer and oligomeric surfactant syntheses of highly ordered, hydrothermally stable, mesoporous silica structures, J. Am. Chem. Soc. 120 (1998) 6024–6036.

[25] X. Yuan, W. Xing, S.P. Zhuo, Z.H. Han, G.Q. Wang, X.L. Gao, Z.F. Yan, Preparation and application of mesoporous Fe/carbon composites as a drug carrier, Micropor. Mesopor. Mater. 117 (2009) 678–684.

[26] Y. Chi, W.C. Geng, L. Zhao, X. Yan, Q. Yuan, N. Li, X.T. Li, Comprehensive study of mesoporous carbon functionalized with carboxylate groups and magnetic nanoparticles as a promising adsorbent, J. Colloid Interface Sci. 369 (2012) 366–372.

[27] Y.Y. Liu, Z.T. Zeng, G.M. Zeng, L. Tang, Y. Pang, Z. Li, C. Liu, X.X. Lei, M.S. Wu, P.Y. Ren, Z.F. Liu, M. Chen, G.X. Xie, Immobilization of laccase on magnetic bimodal mesoporous carbon and the application in the removal of phenolic compounds, Bioresour. Technol. 115 (2012) 21–26.

[28] S. Mor, K. Ravindra, N.R. Bishnoi, Adsorption of chromium from aqueous solution by activated alumina and activated charcoal, Bioresour. Technol. 98 (2007) 954–957.

[29] A. Rao, A. Bankar, A. Ravi Kumar, S. Gosavi, S. Zinjarde, Removal of hexavalent chromium ions by Yarrowia lipolytica cells modified with phyto-inspired Fe^0/Fe_3O_4 nanoparticles, J. Contam. Hydrol. 146 (2013) 63–73.

[30] N.N. Thinh, P.T.B. Hanh, L.T.Th. Ha, L.N. Anh, T.V. Hoang, V.D. Hoang, L.H. Dang, N.V. Khoi, T.D. Lam, Magnetic chitosan nanoparticles for removal of Cr(VI) from aqueous solution, Mater. Sci. Eng. C 33 (2013) 1214–1218.

[31] S. Nethaji, A. Sivasamy, A.B. Mandal, Preparation and characterization of corn cob activated carbon coated with nano-sized magnetite particles for the removal of Cr(VI), Bioresour. Technol. 134 (2013) 94–100.

[32] M. Bhaumik, A. Maity, V.V. Srinivasu, M.S. Onyango, Removal of hexavalent chromium from aqueous solution using polypyrrole–polyaniline nanofibers, Chem. Eng. J. 181–182 (2012) 323–333.

[33] J.S. Li, X.Y. Miao, Y.X. Hao, J.Y. Zhao, X.Y. Sun, L.J. Wang, Synthesis, amino-functionalization of mesoporous silica and its adsorption of Cr(VI), J. Colloid Interface Sci. 318 (2008) 309–314.

[34] B. Geng, Z.H. Jin, T.L. Li, X.H. Qi, Kinetics of hexavalent chromium removal from water by chitosan-Fe^0 nanoparticles, Chemosphere 75 (2009) 825–830.

[35] A.R. Pratt, N.S. McIntyre, Comments on curve fitting of Cr 2p photoelectron spectra of Cr_2O_3 and CrF_3, Surf. Interface Anal. 24 (1996) 529–530.

[36] H.J. Cui, M.L. Fu, S. Yu, M.K. Wang, Reduction and removal of Cr(VI) from aqueous solutions using modified byproducts of beer production, J. Hazard. Mater. 2–3 (2011) 1625–1631.

[37] P.P. Huang, Z.F. Ye, W.M. Xie, Q. Chen, J. Li, Z.C. Xu, M.S. Yao, Rapid magnetic removal of aqueous heavy metals and their relevant mechanisms using nanoscale zero valent iron (nZVI) particles, Water Res. 47 (2013) 4050–4058.

[38] K. Volgmann, F. Voigts, W. Maus-Friedrichs, The interaction of oxygen molecules with iron films studied with MIES, UPS and XPS, Surf. Sci. 604 (2010) 906–913.

[39] P.X. Wu, S.Z. Li, L.T. Ju, N.W. Zhu, J.H. Wu, P. Li, Z. Dang, Mechanism of the reduction of hexavalent chromium by organo-montmorillonite supported iron nanoparticles, J. Hazard. Mater. 219–220 (2012) 283–288.